minerals

MDPI

Article

A Near-Source Electromagnetic Method for Deep Ore Explorations

Guoqiang Xue [1,2,3], Weiying Chen [1,2,3,*], Xin Wu [1,2,3], Shu Yan [4] and Wenbo Guo [5]

1 Key Laboratory of Mineral Resources, Institute of Geology and Geophysics, Chinese Academy of Sciences, Beijing 100029, China
2 College of Earth and Planetary Sciences, University of Chinese Academy of Sciences, Beijing 100049, China
3 Innovation Academy for Earth Science, Chinese Academy of Sciences, Beijing 100029, China
4 School of Computer Science and Communication Engineering, Jiangsu University, Zhenjiang 212013, China
5 Xi'an Geophysical and Geochemical Exploration Co., Northwest Bureau of Geological Non-Ferrous Metals, Xi'an 710068, China
* Correspondence: cwy@mail.iggcas.ac.cn

Abstract: A near-source electromagnetic method known as the short-offset transient electromagnetic (SOTEM) method was proposed. Compared with the traditional far-source methods, the offset of the SOTEM method is greatly reduced, to only 0.3~2 times of the maximum depth. Therefore, the SOTEM can obtain the signal with higher signal-to-noise ratio and sensitivity. Application in the Xiaoshan Mine of Henan Province showed that the SOTEM method is an effective method for deep ore exploration, especially in mountainous areas.

Keywords: grounded-wire source; transient electromagnetics; short-offset; near source; deep ore exploration

check for updates

Citation: Xue, G.; Chen, W.; Wu, X.; Yan, S.; Guo, W. A Near-Source Electromagnetic Method for Deep Ore Explorations. *Minerals* **2022**, *12*, 1208. https://doi.org/10.3390/min12101208

Academic Editor: Michael S. Zhdanov

Received: 13 September 2022
Accepted: 21 September 2022
Published: 25 September 2022

1. Introduction

Electromagnetic (EM) method is one kind of geophysical technique based on the principle of electromagnetic induction. It detects the electrical characteristics and spatial distributions of underground structures by observing and interpreting the responses of the earth excited by natural or artificial electromagnetic sources. Electromagnetic method is the main tool for exploring mineral resources due to its great detection depth and low-cost field work [1]. However, on a global scale, difficult exploration problems have been addressed using electromagnetic methods, with consideration given to achieving both great depths and high precision [2].

The earliest and most mature art of EM sounding is the magnetotelluric (MT) method that was proposed by the former Soviet Union scholar Tikhonov and French scholar Cagniard in the early 1950s [3]. The MT method uses natural electromagnetic fields as the excitation sources, which have the advantages of achieving great exploration depths and simple data processing and interpretation. However, due to random fluctuations in the strength of natural EM fields, the accuracy of the MT method remains low. Consequently, it is generally used in deep structural exploration but less often in the field of mineral resource exploration [4].

In 1971, Canadian researchers established a controlled-source audio magnetotelluric (CSAMT) method [5] using various assumptions and approximations that achieved a historic breakthrough in electromagnetic exploration. It has been found that the introduction of artificial sources can overcome the weak-signal defects of natural sources and improve the strength and controllability of the observed signals. However, the introduction of artificial sources also introduces many problems related to those sources. For example, the calculations and interpretations of electromagnetic fields become more complicated [6]. As a result, the development of methods for determining the geometric relationships between observation points and sources has become a key area of focus. The premise of earth explorations based on traditional electromagnetic theories is that the electromagnetic field signals at delegated observation points should satisfy the plane-wave approximations [7]. This means that current electromagnetic methods using artificial sources require large offsets. For example, approaches such as the CSAMT method in the frequency domain and the long-offset transient electromagnetic (LOTEM) method in the time domain [8] are based on long grounded-wire sources and have long offsets; that is, the resulting signals can be observed in areas far from those sources.

It has been observed that these longer offsets can ensure that the electromagnetic signals satisfy the plane-wave hypothesis and avoid complex field-source effects. As a result, the complexity of the processing and interpretation can be reduced. However, the magnitude of the response signals may decrease with the offset. In addition, as the transmit–receive offset increases, the bandwidths of the signals will narrow to some extent, which tends to limit the maximum detectable depths and the detection resolution levels [9].

Since methods that use distant sources or long offsets are based on mechanisms for detecting plane-wave field sources, the offset problems can essentially be seen as manifestations of the detection mechanisms. That is to say, the above-mentioned problems are caused by the selection of the plane-wave field source detection mechanisms under the conditions of artificial sources [9].

In actual scenarios, the energy levels of electromagnetic fields in near-source regions tend to be strong, making them more suitable for fine detection processes. However, the structures of electromagnetic fields near sources are complex and vary greatly, which makes the exact solutions of the fields and the extraction of the electrical parameters more difficult [10].

To overcome the restrictions of plane-wave field source detection mechanisms in artificial source electromagnetic detection, He [11] proposed a wide-field electromagnetic method (WFEM) based on the exact solution of the electromagnetic field. The WFEM was able to break through the limitations of conventional frequency-domain electromagnetic methods, which can be used only in far-field zones, and reduced the offset to 3 times the skin depth. In addition, within the field of marine controlled-source electromagnetic methods, Ziolkowski [12] put forward a multi-transient electromagnetic method (MTEM) that used an offset of at least two times the maximum detection depth. A great deal of theoretical demonstration and practice in recent years has demonstrated that such near-source EM methods can make full use of the energy and bandwidths of transmitting sources.

This study proposes a short-offset transient electromagnetic (SOTEM) method and compares it to a traditional LOTEM method, with the offsets of the observation points reduced from distances of approximately 4–6 times the depth to approximately 0.3–2 times the depth. This method extends the traditional long-offset mode to a short-offset mode and was found to not only greatly enhance the signal strength of the secondary fields but to also reduce the signal-averaging effects caused by long-distance observations. At the same time, the short-offset observations reduce the requirements for transmitter power, thereby making it more convenient to transmit and receive. In addition, construction efficiency was improved, making the method suitable for applications in mountainous areas [13]. Subsequently, greater detection depths and higher resolution results have been achieved, with smaller offsets further reducing volume effects. In this paper, we firstly give an introduction of the SOTEM method, then illustrate its field application through a case conducted in Henan province, China.

2. Methodology

2.1. Introduction of SOTEM

The SOTEM method uses a ground wire source with bipolar currents to excite the primary electromagnetic fields and uses coil or electrodes to observing the secondary EM fields at the offset that approximately equal to 0.3–2 times of the detection depth (Figure 1).

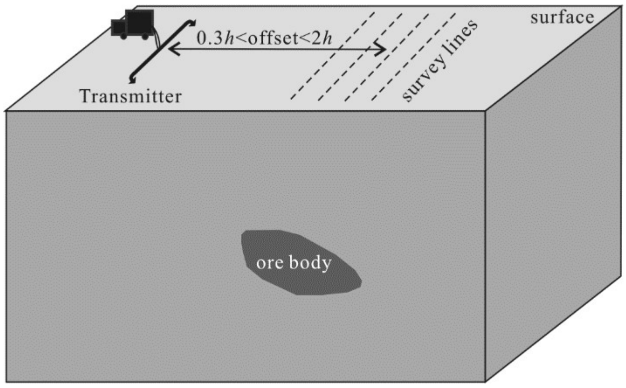

Figure 1. Diagram of SOTEM method. The grounded-wire source is parallel to the survey lines at a distance (offset) of approximately 0.3–2 times the maximum detection depth (*h*).

To achieve greater depths, the traditional LOTEM method requires signal observations with very long time delays. To ensure the strength of late signals at large offsets, continuous bipolar step waves are used to excite the electromagnetic fields [8]. The received signals are then full-waveform responses containing primary fields (Figure 2a). However, it is necessary to consider the effects of the source noise caused by the currents as well as the geological noise caused by the primary fields [14]. To address the noise issues, deconvolution is required to extract the pure impulse responses of the earth. However, it has been found that LOTEM methods cannot be effectively used in areas near the source. When bipolar step waves are used (Figure 2b), the primary fields of the sources disappear soon after the switch-off, and the pure secondary fields induced only by the earth can be obtained near the source areas.

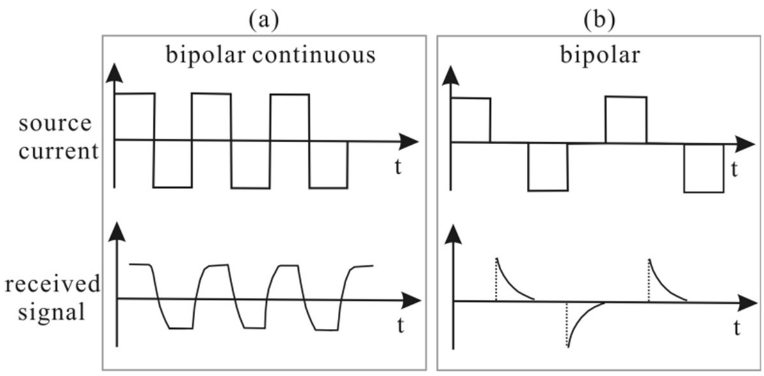

Figure 2. Continuous bipolar and bipolar current forms. (**a**) Bipolar continuous current; (**b**) Bipolar current.

TEM methods make use of these pure secondary fields that remain after the primary fields are turned off. Expressions of the vertically induced voltages excited by a horizontal electric dipole above the uniform half-space model (Formula (1)) showed that when the primary fields were turned off the secondary field signals $\frac{\partial B(t)}{\partial t}$ at any distance from the source contained the electrical information of the underground medium [15]:

$$\frac{\partial B_z(t)}{\partial t} = \frac{3P_E \rho \sin\varphi}{2\pi r^4}\left[\Phi(u) - \sqrt{\frac{2}{\pi}}u(1+\frac{u^2}{3})e^{-u^2/2}\right] \quad (1)$$

where P_E indicates the transmitting magnetic moment; ρ represents the earth's resistivity, φ represents the angle between the receiver and transmitter, r denotes the offset, and $\Phi(u)$ is the probability function:

$$u = \frac{2\pi r}{\tau},\ \tau = 2\pi\sqrt{2\rho t/\mu_0} = \sqrt{2\pi\rho t \times 10^7}.$$

Formula (1) is a complex implicit function of resistivity ρ, from which the explicit expression of resistivity cannot be obtained directly. We then must simplify the formula under certain approximate conditions. In particular, in the far-field zones (early time), ($u >> 1$),

$$\frac{\partial B_z(t)}{\partial t} = \frac{3P_E\rho\sin\varphi}{2\pi r^4}. \tag{2}$$

In the near-field zones (late time), ($u << 1$),

$$\frac{\partial B_z(t)}{\partial t} = -\frac{P_E r\mu_0^{5/2}}{60\pi^{3/2}t^{5/2}\rho^{3/2}}. \tag{3}$$

Using Formulas (2) and (3), it was found that when the observation points were located in far-field zones the electromotive force $\partial B_z/\partial t$ was proportional to the formation ρ, whereas when the observations points were in the near-field zone the electromotive force $\partial B_z/\partial t$ was proportional to the $\rho^{-3/2}$. This indicated that the electromotive forces were more sensitive in the near-source areas.

In the present study, a three-layer model with a low-resistivity middle layer was designed. Then, vertically induced electromotive forces at different offsets were calculated and compared with the responses of the uniform half-spaces (Figure 3). It was observed that even in the case of great buried target depths (d_1 = 2000 m), the electromagnetic field at short offsets (r = 500 m) could still be used to distinguish the underground medium. In addition, when compared with long offsets, the electromagnetic field strength had been significantly improved. Moreover, the maximum relative errors [16] could be used to compare the resolutions with different offsets, as detailed in Table 1. As can be seen in this table, as the offsets increase, the resolution levels of the electromagnetic fields are gradually reduced. Additionally, the volume effects of electromagnetic fields caused by the large offsets have been observed to be more serious under real geological conditions, which tend to further reduce the detection sensitivity [17].

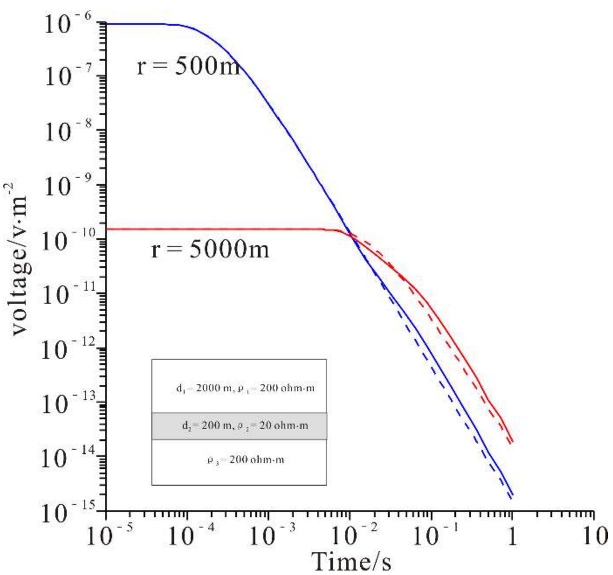

Figure 3. Comparison of responses of three-layer model and half-space model. The solid lines represent the three-layer model and the dashed lines represent the half-space model.

Table 1. Maximum relative errors for different offsets.

Offset (m)	200	500	1000	2000	5000
Error (%)	72.93	69.42	63.66	48.61	25.46

The detection depths of TEM methods are mainly based on the intensities of the signals, the sensitivity of the receiving instruments, noise levels, geoelectric parameters, the positions of the receiving and transmitting points, and so on. In a previous related study, Spies [18] proposed formulas for estimating the maximum detection depths of electrical-source TEM methods under different field conditions as follows:

In far-field areas

$$d_f = 0.28\left(\frac{I\rho AB}{\eta}\right)^{1/4} \tag{4}$$

and in near-field areas

$$d_n = 0.48\left(\frac{Ir\rho AB}{\eta}\right)^{1/5} \tag{5}$$

where η represents the minimum resolvable voltage of the instrument, I indicates the transmission current, and AB is the length of the transmission line.

Based on Formulas (4) and (5), depths detectable under various parameters were calculated, as shown in Table 2. Regardless of the parameter values, the detection depths in the near-field areas were greater than those in the far-field areas. These findings indicate that the detection depths in the near source areas were greater even when the observation times were the same.

Table 2. Detectable depths of the far-area mode and near-area mode at different parameters.

I (A)	**ρ (Ω·m)**	**AB (m)**	**r (m)**	**η (nV)**	**d_f (m)**	**d_n (m)**
5	50	300	200 300	60	526.4	576.5 625.2
10	100	500	300 500	60	845.9	913.7 1012.0
20	300	1000	700 1000	60	1574.5	1779.3 1910.9

2.2. Data Inversion

An adaptive regularized inversion algorithm (ARIA) was adopted in this study [19]. A brief description of the ARIA is given below.

In this study, both the errors in the data fitting and the model roughness were taken into account. Meanwhile, a regularized inversion algorithm was constructed, with the total objective function containing both the data objective function $\mathbf{\Phi_d}$ and the model objective function $\mathbf{\Phi_m}$ as follows:

$$\mathbf{\Phi} = \mathbf{\Phi_d} + \lambda\mathbf{\Phi_m} \rightarrow \min \tag{6}$$

where $\mathbf{\Phi_d} = (\mathbf{d} - \mathbf{A}(\mathbf{m}))^T\mathbf{W_d}(\mathbf{d} - \mathbf{A}(\mathbf{m}))$ is the data objective function; $\mathbf{\Phi_m} = \mathbf{m}^T\mathbf{Cm}$ is the model objective function; and λ denotes the weight factor (for example, the regularization adjustment factor). Then, the above equation was rewritten as follows:

$$\mathbf{\Phi} = [\mathbf{d} - \mathbf{A}(\mathbf{m})]^T\mathbf{W_d}[\mathbf{d} - \mathbf{A}(\mathbf{m})] + \lambda\mathbf{m}^T\mathbf{mCm} \tag{7}$$

where $\mathbf{d}$ is the observed data vector; $\mathbf{A}(\mathbf{m})$ represents the forward data vector of the model $\mathbf{m}$; $\mathbf{W_d}$ is the covariance matrix of the data; and $\mathbf{C}$ indicates the smoothness matrix of the model.

Then, in accordance with the minimization principle of objective functions, the inversion matrix equation was as follows:

$$\mathbf{W_d J} + \lambda \mathbf{C}\Delta\mathbf{m} = \mathbf{W_d}\Delta\mathbf{d} + \lambda\mathbf{Cm} \tag{8}$$

where $\mathbf{J}$ represents the partial derivative matrix of the forward data to the model.

Therefore, the model of every iteration can be written as: $m_{i+1} = m_i + \Delta m$.

In order to ensure that during the inversion process, there was basically no relationship between the value of the data objective function and the data error, the data variance was normalized as follows [19]:

$$\mathbf{W_d} = \frac{\Delta\mathbf{d}^T\Delta\mathbf{d}}{\Delta\mathbf{d}^T\boldsymbol{\sigma}_0^d\Delta\mathbf{d}}\boldsymbol{\sigma}_0^d \tag{9}$$

where $\boldsymbol{\sigma}_0^d$ is the covariance matrix of the observed data, and its specific expression was:

$$\boldsymbol{\sigma}_0^{d_i} = \begin{cases} 0.0 & \varepsilon_i \geq 1.0 \\ 1.0 - \varepsilon_i & \varepsilon_i < 1.0 \end{cases} \tag{10}$$

where ε_i is the relative error of the observed data. As a result, the covariance matrix element could be controlled between 0 and 1. In addition, when the data error is large, the penalty should be relatively large, with its contribution to the objective function relatively weakened or even removed during the inversion process. Otherwise, the opposite would occur.

In regular inversion processes, such as Occam's inversion [20], the regularization factor is minimized in each iteration, which means that inversion equations are required to be repeatedly solved during the process. Therefore, in order to reduce the calculations, according to the relationship between the data objective function and the model objective function, an adaptive regularization adjustment factor is introduced as follows [19]:

$$\lambda_k = \frac{\Phi_d^{k-1}}{\Phi_d^{k-1} + \Phi_m^{k-1}} \tag{11}$$

3. Case History

SOTEM methods have been successfully applied in many deep-mining explorations in China. This research investigation selected the Xiaoshan Mine explorations as examples to illustrate the use of these methods. The Xiaoshan area is located in the south margin of northern China, adjacent to Xiaoqinling and the Xiongershan area. It is in adjacent area of the East Qinling and Northern China Craton mountains (Figure 4). The geology is mainly metamorphic core complex rock. This area is characterized by a superior metallogenic geologic background following many long and complex periods of geologic evolution [21]. The Xiaoshan area has been considered to have major potential for metal exploration in western China, but thus far there have been only a few successful detections. The geological evidence reveals that the denudation and unroofing of the area are far lower than those of the Xiongershan area. Consequently, the majority of metal resources are buried beyond exploration depths in the Xiaoshan area. The undulating topography in mountainous areas has widely exposed bedrock at the surface, which has limited the applications of traditional geophysical exploration processes and increased the difficulty of prospecting and discovery [22].

In the present study, to investigate the positions and shapes of electrical structures in the area to a depth of up to 1000 m and to delineate the position of the anomaly body, SOTEM measurements were carried out in an area considered favorable for ore formations based on available geological data. In this work, four survey lines were arranged, and a 1-km transmitting line was laid out along a mountain path (Figure 5). The V8 electromagnetic system provided by the Phoenix Company of Canada was used to transmit and receive the electromagnetic signal. The transmitting current was 16 A with a base frequency of 2.5 Hz. A magnetic probe with an effective area of 40,000 m^2 was used to record the vertical induced voltage. The quality of the raw observed data is high because of the small Tx-Rx offset and the low level of electromagnetic interference in the measuring area. Figure 6 shows the raw multi-channel curves of L3 (Figure 6a) and L4 (Figure 6b).

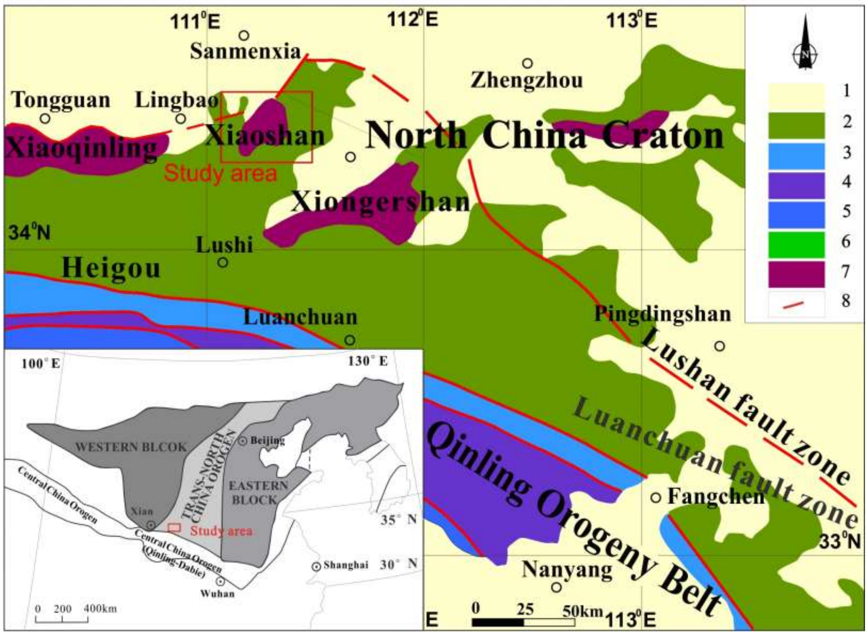

Figure 4. Geological map of the survey area [20]. (1) Quaternary; (2) Cover strata of the North China Craton; (3) Kuanping Group; (4) Erlangping Group; (5) Qinling Group; (6) South Qingling sequences; (7) Archean metamorphic rock; (8) Regional principal fault.

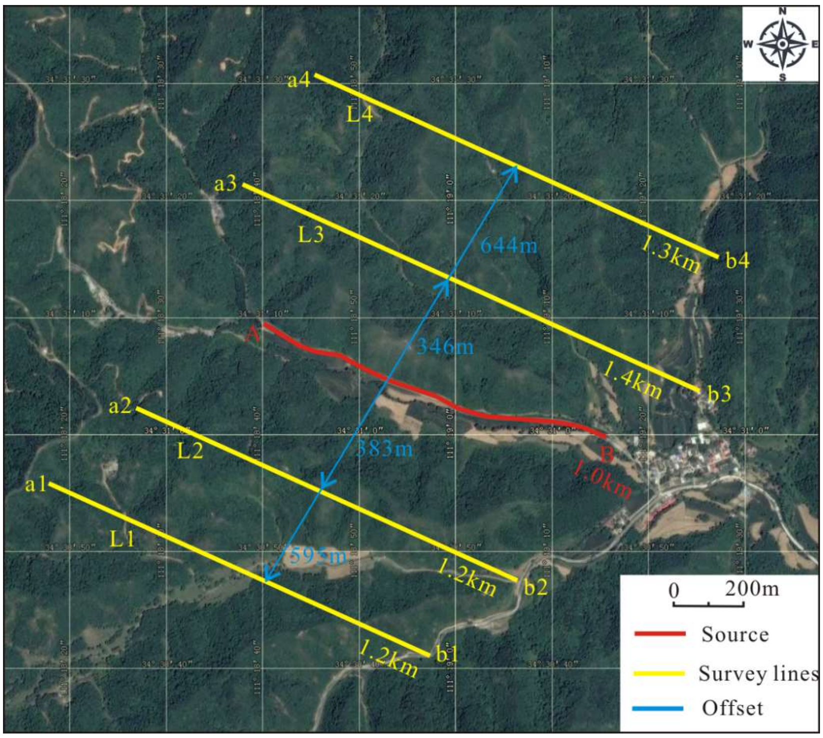

Figure 5. Layout of the transmitting source and survey lines.

Following the denoising and inversion of the measured data [21], the researchers obtained the elevation–resistivity cross section of each survey line. Taking Line 3 as an example (Figure 7), it was observed that the resistivity levels of the shallow areas were low, while those of the deeper areas were higher, which is consistent with the Quaternary sedimentary layers and the alerted rocks in the shallow areas and conditions of the mixed granite rock of the Taihua Group. It was also observed that between 300 m and 600 m along Line 3, the high resistivity stratum extended from the deep areas to the shallow areas, which was highly consistent with the geological model [19] provided by Liu et al. These results indicate that the Taihua Group was uplifted to the surface in those areas, and the Xionger Group at the top had been denuded. In addition, between the two stratums, faults F1 and F2 were determined to be the causes of the low-resistivity reflections. Combining these observations with the data on the ore structures and occurrence laws, this study speculated that there may have been a large range of mineralization anomalies near F2 fault. To verify this, three boreholes (Drill 1 to Drill 3) were sunk on Line 3. The boreholes designated as Drill 1 and Drill 2 also identified two layers of metal resources at a depth of 800 m.

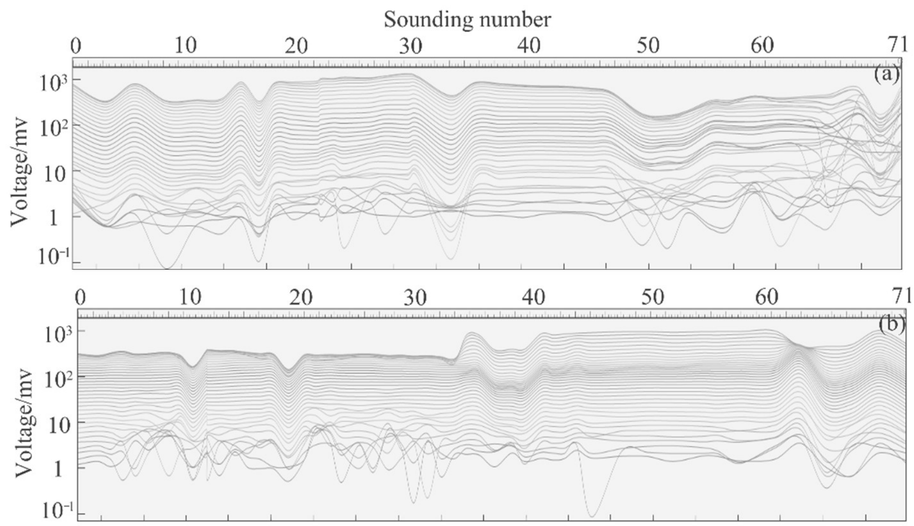

Figure 6. Multi-channel curves of L3 (**a**) and L4 (**b**).

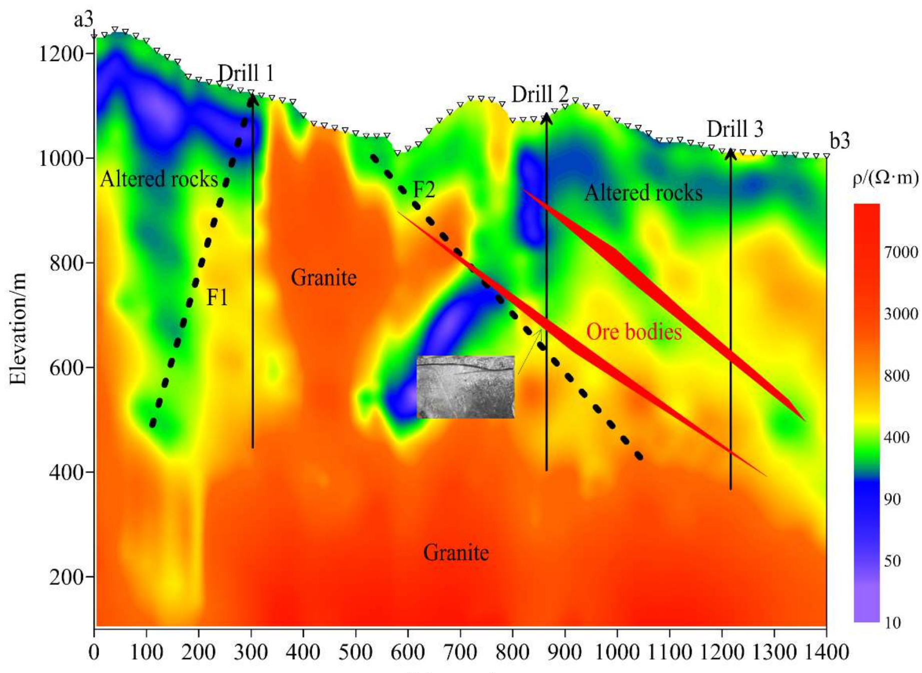

Figure 7. Elevation-resistivity cross section and interpretations along Line 3. The inverted triangles represent the location of the measurement points.

Finally, the inversion results of all the lines are shown together, as shown in Figure 8. It can be seen that the electrical structure of the strata revealed by the four lines is similar to a certain extent, the high resistivity granite basement has a good continuity, the F2 fault traverses the four lines, while the F1 fault is only shown on the L3 and L4 lines. The general shape and extension of the orebodies are plotted according to the location of the orebody revealed by drills on the survey lines. This is consistent with the result inferred from the inversion resistivity profile.

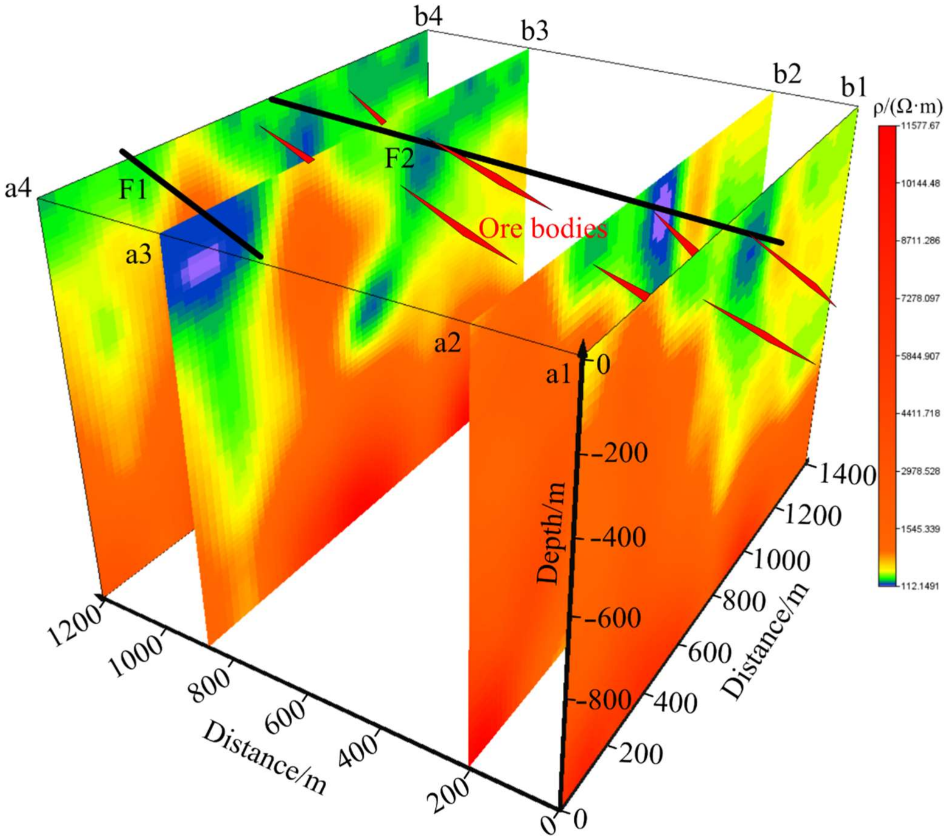

Figure 8. Depth–resistivity cross section of four survey lines.

4. Conclusions

The traditional artificial-source TEM methods are based on a plane-wave approximation theory and require long offsets, resulting in weak signals and low resolution. In actual on-site situations, sounding in the near-source areas can be feasible using appropriate transmitting waveforms and observational means. SOTEM methods apply discontinuous square wave currents using long grounded-line sources and short offsets within two times the detection depths to observe pure secondary field signals. In this study, the feasibility and superiority of SOTEM methods were firstly verified, and then a case history conducted in Xiaoshan Henan province was introduced to show the practical application of SOTEM. The results showed that the SOTEM methods had the advantages of high detection accuracy, large detection depths, convenient and efficient construction, and suitability for applications in mountainous areas. Therefore, this study concludes that the use of SOTEM methods is appropriate for deep mineral resource exploration.

Author Contributions: G.X.: conceptualization, methodology, writing—original draft preparation; W.C.: data acquisition, data processing, writing—review and editing; X.W.: software, validation; S.Y.: formal analysis, investigation; W.G.: data acquisition, supervision. All authors have read and agreed to the published version of the manuscript.

Funding: This research was funded by National Natural Science Foundation of China (42030106, 42274192), the second Tibetan Plateau Scientific Expedition and research Program (2019QZKK0804), the Key Deployment Project of Institute of Geology and Geophysics, Chinese Academy of Sciences (IGGCAS-201901), the Scientific Equipment Instrument and Development Project of the Chinese Academy of Sciences (YJKYYQ20190004).

Data Availability Statement: The data used to support the findings of this study are available with the corresponding author upon request.

Conflicts of Interest: The authors declare that they have no known competing financial interests or personal relationships that could have appeared to influence the work reported in this paper. The authors declare no conflict of interest.

References

1. Teng, J.W. Strengthening exploration of metallic minerals in the second depth space of the crust, accelerating development and industrialization of new geophysical technology and instrumental equipment. *Prog. Geophys.* **2010**, *25*, 729–748.
2. Di, Q.Y.; Zhu, R.X.; Xue, G.Q.; Yin, C.; Li, X. New development of the Electromagnetic (EM) methods for deep exploration. *Chin. J. Geophys.* **2019**, *62*, 2128–2138.
3. Cagniard, L. Basic theory of the magneto-telluric method of geophysical prospecting. *Geophysics* **1953**, *18*, 605–635. [CrossRef]
4. Di, Q.Y.; Xue, G.Q.; Fu, C.M.; Wang, R. An alternative tool to controlled-source audio-frequency magnetotellurics method for prospecting deeply buried ore deposits. *Sci. Bull.* **2020**, *65*, 611–615. [CrossRef]
5. Goldstrein, M.A.; Strangway, D.W. Audio-frequency magnetotellurics with a grounded electric dipole source. *Geophysics* **1975**, *40*, 669–683. [CrossRef]
6. Zhou, N.N.; Xue, G.Q.; Hou, D.Y.; Lu, Y. An investigation of the effect of source geometry on grounded-wire TEM surveying with horizontal electric field. *J. Environ. Eng. Geophys.* **2018**, *23*, 143–151. [CrossRef]
7. Nabighian, M. *Electromagnetic Methods in Applied Geophysics (Volume 2)*; Society of Exploration Geophysicists: Tulsa, OK, USA, 1991.
8. Strack, K.M. *Exploration with Deep Transient Electromagnetic Method*; Elsevier: New York, NY, USA, 1992.
9. He, J.S.; Xue, G.Q. Review of the key techniques on short-offset electromagnetic detection. *Chin. J. Gephys.* **2018**, *61*, 1–8.
10. Xue, G.Q. The Development of near-source electromagnetic methods in China. *J. Environ. Eng. Geophys.* **2018**, *23*, 115–124. [CrossRef]
11. He, J.S. *Wide-Field Electromagnetic Method and Pseudo-Random Signal*; Higher Education Press: Beijing, China, 2010. (In Chinese)
12. Ziolkowski, A.; Hobbs, B.A.; Wright, D. Multi-transient electromagnetic demonstration survey in France. *Geophysics* **2007**, *72*, 197–209. [CrossRef]
13. Xue, G.Q.; Chen, W.Y.; Zhou, N.N.; Li, H. Short-offset TEM technique with a grounded wire source for deep sounding. *Chin. J Geophys.* **2013**, *56*, 255–261.
14. Niu, Z.L. *Principle of Time-Domain Electromagnetic Method*; Central South University Press: Changsha, China, 2007. (In Chinese)
15. Kaufman, A.A.; Keller, G.V. *Frequency and Transient Soundings*; Elsevier: New York, NY, USA, 1983.
16. Chen, W.Y.; Xue, G.Q.; Cui, J.Y. Study on the response and optimal observation area for SOTEM. *Chin. J. Geophys.* **2016**, *59*, 739–748.
17. Hördt, A.; Druskin, V.L.; Kinizhnerman, L.A.; Strack, K.M. Interpretation of 3-D effects in long-offset transient electromagnetic (LOTEM) soundings in the Munsterland area/Germany. *Geophysics* **1992**, *57*, 1127–1137. [CrossRef]
18. Spies, B.R. Depth of investigation in electromagnetic sounding methods. *Geophysics* **1989**, *54*, 872–888. [CrossRef]
19. Chen, X.; Zhao, G.; Tang, J.; Zhan, Y.; Wang, J.J. A adaptive regularized inversion algorithm for magnetotelluric data. *Chin. J. Geophys.* **2005**, *48*, 937–946. (In Chinese) [CrossRef]
20. Constable, S.C.; Parker, R.L.; Constable, C.G. Occam's inversion—A practical algorithm for generating smooth models from electromagnetic sounding data. *Geophysics* **1987**, *52*, 289–300. [CrossRef]
21. Liu, H.T.; Di, Q.Y.; Xue, G.Q.; Luo, X.N.; Ding, Y.H.; Wang, C.Y. The metamorphic core complex in the Xiaoshan gold-polymetallic concentrating area of Henan Province and its implications for mineral exploration. *Geol. Explor.* **2018**, *54*, 230–242.
22. Xue, G.Q.; Zhang, L.B.; Hou, D.Y.; Liu, H.T.; Ding, Y.H.; Wang, C.Y.; Luo, X.N. Integrated geological and geophysical investigations for the discovery of deeply buried gold-polymetallic deposits in China. *Geol. J.* **2020**, *55*, 1771–1780. [CrossRef]